

Photon statistics characterization of a single-photon source

R Alléaume¹, F Treussart^{1,3}, J-M Courty² and J-F Roch¹

¹ Laboratoire de Photonique Quantique et Moléculaire, Laboratoire du CNRS, UMR 8537, associé à l'École Normale Supérieure de Cachan, ENS Cachan, 61 avenue du président Wilson, 94235 Cachan cedex, France

² Laboratoire Kastler Brossel, UMR 8552, Unité mixte de recherche de l'École Normale Supérieure, du CNRS, et de l'Université Pierre et Marie Curie, UPMC case 74, 4 place Jussieu, 75252 Paris cedex 05, France

E-mail: francois.treussart@physique.ens-cachan.fr

New Journal of Physics **6** (2004) 85

Received 9 December 2003

Published 29 July 2004

Online at <http://www.njp.org/>

doi:10.1088/1367-2630/6/1/085

Abstract. In a recent experiment, we reported the time-domain intensity noise measurement of a single-photon source relying on single-molecule fluorescence control. In this paper, we present data processing starting from photocount timestamps. The theoretical analytical expression of the time-dependent Mandel parameter $Q(T)$ of an intermittent single-photon source is derived from ON \leftrightarrow OFF dynamics. Finally, source intensity noise analysis, using the Mandel parameter, is quantitatively compared with the usual approach relying on the time autocorrelation function, both methods yielding the same molecular dynamical parameters.

³ Author to whom any correspondence should be addressed.

Contents

1. Introduction	2
2. Single-photon emission from a single molecule	3
2.1. Principle of the experiment	3
2.2. Experimental set-up	4
2.3. Data acquisition	5
3. Single-pulse photon statistics	7
3.1. Influence of deadtime	7
3.2. Calibration with a coherent source	8
3.2.1. Coherent beam photocount statistics	8
3.2.2. Experimental calibration	9
3.3. Molecular SPS efficiency	9
3.4. Single-pulse Mandel parameter	10
4. SPS intensity fluctuations	11
4.1. Measuring intensity fluctuations: time-varying Mandel parameter $Q(T)$	12
4.2. Intensity noise and intermittency in the molecular fluorescence: the ON–OFF model	12
4.2.1. Physical interpretation of the ON–OFF model	12
4.2.2. Dynamics of the ON–OFF system	13
4.2.3. Source intensity and Mandel parameter versus time	14
4.2.4. Experimental data analysis	14
4.2.5. SPS intensity autocorrelation function	15
5. Conclusion	16
Acknowledgments	17
Appendix A. General analysis technique of a set of photocounts	17
Appendix B. Statistical characterization of an intermittent SPS	20
Appendix C. Histogram of time delays from the set of photocounts	21
References	23

1. Introduction

Optical experiments at the level of single quantum emitters allow one to produce specific quantum states of light with photon statistics that deviate strongly from classical distributions [1, 2]. Despite the experimental challenges of producing single-photon states [3, 4], recent developments of quantum information theory have intensified interest in single-photon sources (SPSs). Realization of an efficient SPS is, for instance, a key problem in quantum cryptography and could more generally be applied to quantum information processing [5].

Recent experiments reported quantum key distribution (QKD) with polarization encoding on single photons [6, 7]. They revealed the potential gain of such sources over systems relying on strongly attenuated laser pulses. However, in these experiments, the actual performance of QKD is intrinsically linked to photon statistics of the SPS [8].

Following the proposal of De Martini *et al* [9, 10], we recently realized a SPS based upon pulsed excitation of a single molecule [11]. Among various experimental realizations of SPSs

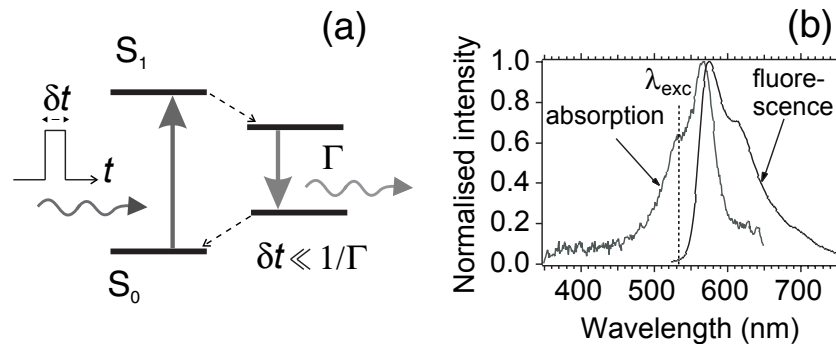


Figure 1. (a) Single-photon generation by pulsed excitation of a single four-level molecular system from the ground singlet state S_0 to a vibrationally excited sublevel of the singlet state S_1 . Solid arrows correspond to optical transitions, whereas dashed arrows depict non-radiative fast (ps) de-excitation. To emit a single photon per excitation pulse, the pulse duration δt must be much shorter than the radiative lifetime $1/\Gamma$. (b) Absorption and fluorescence spectra of DiIC₁₈(3) dye embedded in a thin polymer film, measured respectively with absorption spectrometer and spectrofluorimeter with 514 nm excitation wavelength. Note that in the SPS experiment, the 532 nm excitation wavelength is well separated from the dye's fluorescence emission which is centred at a wavelength around 570 nm.

[12]–[25], a molecular-based SPS presents several advantages. Firstly, it can be driven at room temperature with a relatively simple set-up, which achieves global efficiency exceeding 5% for single-photon production and detection. Secondly, since the molecular fluorescence lifetime is a few nanoseconds, a high repetition rate can potentially be used. Finally, background-emitted photon intensity level is extremely low for carefully prepared samples.

At the single-pulse timescale, the figure of merit of an SPS can be characterized by efficiency of delivering triggered photons to target and by the ratio of single-photon to multiphoton pulses [10]. In [11], we extended this analysis to measurement of SPS noise properties over a wide integration timescale range. In the detection scheme, complete statistical information is extracted from the ‘photon count by photon count’ record. We have shown that measured photon statistics strongly deviates from the Poisson law, clearly exhibiting non-classical features.

In this paper, we detail the steps of this work from realization of a molecular-based SPS to extensive statistical analysis of detected photons.

2. Single-photon emission from a single molecule

2.1. Principle of the experiment

As fluorescence light of a four-level single emitter is anti-bunched for a timescale of the order of the excited state radiative lifetime [14], [26]–[28], such systems can simply produce single photons on demand [9, 10, 13]. As summarized in figure 1, the molecule is pumped into a vibrational excited state by a short excitation pulse. It then quickly decays to the first electronic excited state by a non-radiative process [29]. The emission of a single fluorescence photon

then coincides with radiative de-excitation towards the ground-state vibrational multiplicity, followed once again by fast non-radiative decay (figure 1). To emit more than one photon at a time, a molecule has to undergo a full excitation, emission and re-excitation cycle within the same excitation pulse. The probability of this occurrence is extremely small when the pulse duration is much shorter than the excited-state lifetime [9, 10]. Following the theoretical analysis of Brouri *et al* [10], we chose a pulse duration of $\simeq 150$ fs, which makes this probability less than 5×10^{-5} . This value is negligible in comparison with the one associated with parasitic light, such as residual fluorescence from the molecular host matrix. To get one fluorescent photon per excitation pulse, the repetition period must also be much longer than the excited-state lifetime so as to ensure relaxation into the ground state before application of the next excitation pulse.

2.2. Experimental set-up

We use standard confocal microscopy techniques to perform selective excitation and detection of single-molecule light emission at room temperature [28]. This set-up allows one to readily achieve two required features for observation of non-classical photon statistics, namely good collection efficiency of emitted photons and high rejection of optical background noise.

The laser source, used for fluorescence excitation, is a fs-tunable titanium : sapphire (Ti : Sa) laser, frequency-doubled by single-pass propagation into a LiIO_3 non-linear crystal. The initial repetition rate of 82 MHz is divided by a pulse picker with frequency set to 2.05 MHz (pulsed excitation repetition period $\tau_{\text{rep}} = 488$ ns) to avoid surpassing the maximum electronics counting rate (see figure 2).

The excitation light, centred at 532 nm, is reflected by a dichroic mirror into an inverted microscope. It is focused on the sample with an oil-immersion high numerical aperture objective, leading to a spot diameter of $\simeq 350$ nm FWHM. The fluorescence light—red-shifted with respect to the excitation—is collected by the same objective, then transmitted through the dichroic mirror and finally focused inside a pinhole for the confocal configuration. After recollimation, residual excitation light is removed by a holographic notch filter.

The samples used in our experiment consist of cyanine molecules $\text{DiIC}_{18}(3)$. This dye choice was motivated by its fluorescence efficiency and photostability, with an emission spectrum well suited for detection using a silicon avalanche photodiode (see figure 1(b)). The dye molecules are embedded in a thin layer of PMMA deposited on a microscope coverplate by spin coating. The emitters are randomly distributed within the PMMA layer (thickness $\simeq 30$ nm) at an approximate concentration of 1 molecule per $10 \mu\text{m}^2$.

To ensure localization of a single emitter in the detection volume, we use a standard Hanbury Brown and Twiss set-up [30]. It consists of two single-photon-counting avalanche photodiodes (SPADs) placed on each side of a 50/50 non-polarizing beamsplitter. A start-stop technique with a time-to-amplitude converter allows us to build a coincidences histogram as a function of time delay between two consecutive photodetections on each side of the beamsplitter. Following the textbook experiment of Grangier and Aspect on quantum properties of single-photon states [31], the absence of coincidence at zero delay gives clear evidence of single-photon emission [12].

We hence apply a simple three-step procedure as explained in [11]. We first raster-scan the sample at low energy per pulse ($\simeq 0.5$ pJ) so as to map the fluorescence intensity and locate efficient emitters. We then put the excitation beam on a given emitter and measure

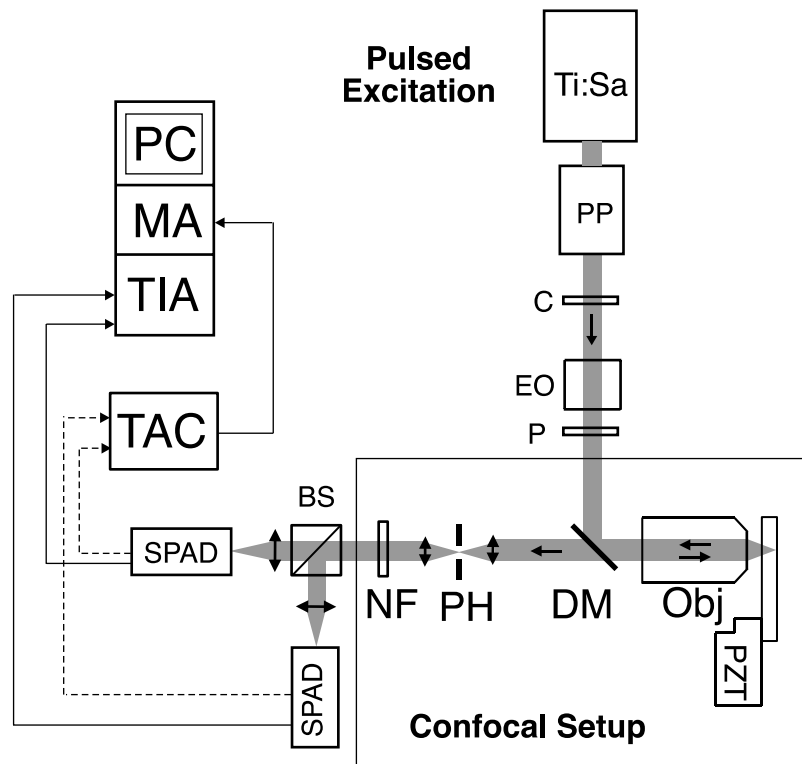


Figure 2. Experimental set-up for characterization of the triggered SPS. Single molecules are excited by a frequency-doubled fs Ti : Sa laser at 532 nm. The laser is followed by PP, pulse picker; C, LiIO₃ non-linear $\chi^{(2)}$ crystal; EO, ADP(NH₄PO₄) electro-optic cell; P, linear polarizer; PZT, piezoelectric translation stage; Obj, oil-immersion microscope objective (60 \times , NA = 1.4); DM, dichroic mirror; PH, pinhole for confocal detection (30 μ m diameter); NF, notch filter centred at 532 nm; BS, non-polarizing beamsplitter; SPAD, single-photon silicon avalanche photodiode; TAC, time-to-amplitude converter; MA, multichannel analyser; TIA, time interval analyser (GuideTech, Model GT653); PC, computer.

the autocorrelation function at low excitation energy. We hence determine whether a single fluorophore or an aggregate of several molecules is excited. Once such preliminary identification has been achieved, the single molecule is excited at much higher power so as to ensure saturated emission [11].

2.3. Data acquisition

Once a single emitter is located, we switch the detection procedure from the start–stop method to a complete recording of photon arrival times. The properly normalized interval function $c(\tau)$ measured by the start–stop technique corresponds to the intensity autocorrelation function $g^{(2)}(\tau)$ in the limit of short timescales and low detection efficiency [32]. However, to characterize more completely the statistical properties of the photon stream, one needs to test for correlations on timescales much longer than the excitation repetition period τ_{rep} . In that case, the relationship

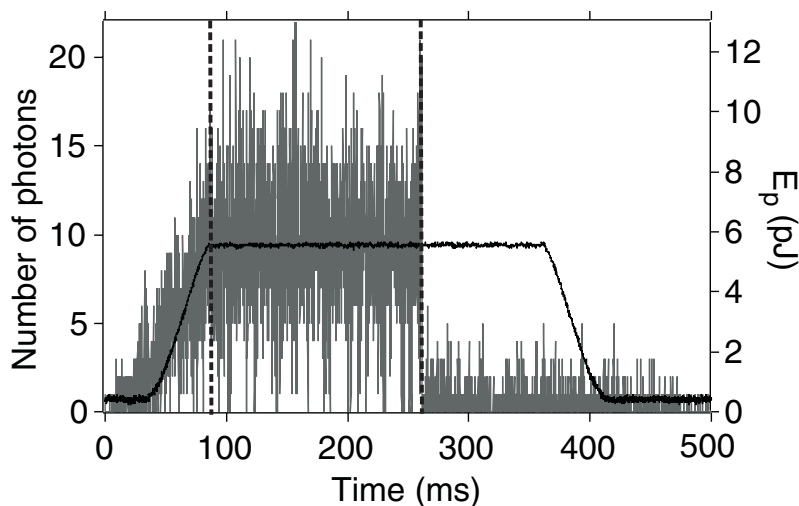


Figure 3. Black solid line (right scale): laser pulse energy E_p versus time during single-molecule excitation. Maximum laser pulse energy E_p^{\max} of 5.6 pJ saturates the molecular transition. Gray solid line (left scale): number of fluorescent photons detected during $50 \mu\text{s}$ integration duration. Photobleaching of the dye occurs 162 ms after excitation at the maximum energy per pulse begins, as delimited by two broken vertical lines.

between $g^{(2)}(\tau)$ and $c(\tau)$ becomes more complicated [32, 27]. Instead of solely inferring $g^{(2)}(\tau)$ from $c(\tau)$ measurements, we have chosen to keep trace of the full range of dynamics by recording every photodetection time with a time interval analyser (TIA) computer board. From this set of photocounts moments (that we call timestamps), detected photons statistics can then be directly analysed over a wide range of timescales. Such a procedure avoids any mathematical bias in photon statistics analysis.

The total number of fluorescence photons that can be produced by a single molecule is limited at room temperature by its photostability [34]. Under weak CW excitation, a molecule of DiIC₁₈(3) typically undergoes 10^6 excitation cycles before irreversible photobleaching occurs [35]. In our experiment, the excitation pulse energy is progressively ramped up to a maximum value of 5.6 pJ that ensures saturation of the $S_0 \rightarrow S_1$ transition [11]. This energy ramp, realized using an electro-optic modulator, consists of a 50 ms linear rise followed by a plateau lasting 300 ms and linear decrease (figure 3). We found experimentally that applying such a procedure substantially improves molecular photostability, compared with an abrupt excitation. We then select the timestamps of photocounts that occurred during the plateau of the excitation. These events correspond to saturated emission of our molecular SPS. Our analysis ‘photocount by photocount’ then relies on determination of the number of detected photons in gated windows synchronized on Ti:Sa excitation pulses.

Data are first pre-processed over a discrete time grid. The excitation time base is reconstructed from the timestamps ensemble $\{t_i\}$ by applying a time filtering procedure described in appendix A. The gate duration is 30 ns, more than 10 times the typical radiative lifetime of the molecule in the PMMA layer. All records outside the time gates are rejected, slightly improving the signal-to-background ratio. Each timestamp t_i is then attributed to a pulse p_i in the time grid, and to each excitation pulse p , a number $n_p^{(d)} = 0, 1, 2$ of detected photons is

Table 1. Single-pulse statistics of a molecular SPS, as obtained after numerical synchronization (see appendix A). These data will be referred to as (S). The total number of excitation pulses in the sequence is 325313, leading to a total of 0, 1 or 2 photon number events of 15138. The mean number of photons detected per pulse is $\langle n \rangle = 0.04653$. No events with $n^{(d)} > 2$ are observed due to deadtime in each detection channel.

$n^{(d)}$ (number of detected photons)	0	1	2
$n^{(d)}$ -photon event number	310190	15108	15
$n^{(d)}$ -photon event probability	0.95351	0.04644	4.6×10^{-5}

finally associated. The probability distribution of the number of detected photons per pulse is deduced from $\{n_p^{(d)}\}$, as summarized in table 1.

We next analyse the photon statistics of a data set extracted from SPS emission displayed in figure 3. We have selected photocounts recorded between the plateau beginning and molecular photobleaching clearly identified by a sudden drop in fluorescence emission. During this time, the molecule was excited at constant maximum pumping energy, yielding 15332 photodetection events for 325313 excitation pulses. The time filtering mentioned above is then applied keeping 15138 synchronous photocounts.

3. Single-pulse photon statistics

The single-pulse statistics, presented in table 1, are the direct outcome of photocounts acquisition. They correspond to the molecular emission displayed in figure 3. While our SPS photon statistics appear to differ from a classical Poissonian distribution, the influence of our experimental set-up on these measurements must be considered for accurate interpretation of these figures and for comparison with Poisson shotnoise reference.

3.1. Influence of deadtime

In the following, we make a distinction between the distribution of the photons produced by the source, denoted by script notation (\mathcal{P}), and photocount statistics, for which we conserve the usual notation (P).

Due to existence of a $\simeq 280$ ns deadtime for each detection channel, a non-linear relationship exists between detected photon statistics and source photon statistics. Indeed, for a given excitation pulse, the number of detected photons in a 30-ns gated time window cannot exceed 2 if we use two avalanche photodiodes (APDs) operating in the photon counting regime compulsory for our experiment.

Denoting by $\mathcal{P}^{\text{in}}(n)$ the photon number probability distribution of incoming light on the detection set-up, the non-linear transformation relating this probability to the *detected* photon probability $P(n = 0, 1, 2)$ is simply computed for ‘ideal APDs’. By ‘ideal APD’, we mean that each photodiode clicks with 100% efficiency immediately upon receiving a photon, but that no more than one click can occur in a given repetition period. In the approach developed here,

we consider the ideal APD case for the following reasons:

- limited quantum efficiency of the APD (65% in our experiment) is included in an overall linear loss coefficient along with other linear losses of the detection chain.
- deadtime is shorter than repetition period τ_{rep} and much longer than pulse duration.

For detection with a single ideal APD, the relationship between the photocount and incoming light statistics is

$$P(0) = \mathcal{P}^{\text{in}}(0) \quad \text{and} \quad P(1) = \sum_{n \geq 1}^{\infty} \mathcal{P}^{\text{in}}(n). \quad (1)$$

With our experimental detection scheme, random splitting of photons on two sides of 50/50 beamsplitter gives

$$P(0) = \mathcal{P}^{\text{in}}(0), \quad (2)$$

$$P(1) = \sum_{n \geq 1}^{\infty} \mathcal{P}^{\text{in}}(n) \frac{1}{2^{n-1}}, \quad (3)$$

$$P(2) = \sum_{n \geq 2}^{\infty} \mathcal{P}^{\text{in}}(n) \left(1 - \frac{1}{2^{n-1}}\right). \quad (4)$$

The relationship between $P(n)$ and photon statistics $\mathcal{P}(n)$ in SPS emission comes from accounting for linear attenuation between SPS and detection. We call η the overall detection efficiency, which includes all linear propagation losses and photodetector quantum efficiency. \mathcal{P}^{in} is then related to \mathcal{P} by the following binomial law:

$$\mathcal{P}^{\text{in}}(n) = \sum_{m=n}^{\infty} \binom{m}{n} \eta^n (1 - \eta)^{m-n} \mathcal{P}(m). \quad (5)$$

Combination of equations (2)–(5) leads to a direct analytical relation between $\mathcal{P}(n)$ and $P(n = 0, 1, 2)$.

Note that the existence of such a saturation limit, due to detection deadtime, has no influence on photocount statistics of a perfect SPS, for which $\mathcal{P}(n \geq 2) = 0$, as long as the excitation repetition period is longer than the electronics deadtime. In contrast, for a ‘real’ source with background light, the number of detected multi-photon pulses is systematically underestimated. It leads to an artificial reduction of intensity noise in comparison with shotnoise reference.

3.2. Calibration with a coherent source

3.2.1. Coherent beam photocount statistics. SPS performance can be directly evaluated by comparing single-pulse photon statistics with those of a coherent source. This calibration takes into account the linear and non-linear effects of our detection set-up and permits accurate measurements of the multi-photon event probability reduction between single-photon and Poissonian sources.

Table 2. Photocount probabilities $P(n)$ for SPS (S), reference experimental coherent source (R) and theoretical coherent source (C), for which photocount statistics are affected by detection. The mean number $\langle n \rangle$ of detected photons per pulse is also given.

	$n = 1$	$n = 2$	$\langle n \rangle$
$P_S(n)$	0.04644	4.6×10^{-5}	0.04653
$P_R(n)$	0.04520	50×10^{-5}	0.04620
$P_C(n)$	0.04514	53×10^{-5}	0.04620

The photon number probability distribution for a coherent pulsed beam (C) is given by a Poisson law. According to equation (5), linear loss between the source and APDs change the mean photon number per pulse α to $\eta\alpha$, whereas the photon statistics remain Poissonian. The expected photocount statistics can then be calculated by applying non-linear transformations (equations (2)–(4)) to a Poissonian distribution of parameter $\eta\alpha$

$$P_C(0) = e^{-\eta\alpha}, \quad (6)$$

$$P_C(1) = 2e^{-\eta\alpha/2}(1 - e^{-\eta\alpha/2}), \quad (7)$$

$$P_C(2) = (1 - e^{-\eta\alpha/2})^2, \quad (8)$$

such distribution being termed as $P_C(n)$ in table 2.

3.2.2. Experimental calibration. A strongly attenuated pulsed laser beam is used as experimental reference to mimic a pulsed coherent source. It is obtained by slightly detuning the Ti:Sa wavelength from the notch filter rejection band resulting in detection of residual pump light reflected from the sample. The photocount statistics of this experimental reference (R) are then compared both with the experimental SPS (S) and the calculated photocount distribution expected from a Poissonian source (C). To establish a valid comparison, calculated and experimental calibrations are determined for an almost identical mean number of photons detected per pulse.

Table 2 shows that theoretical predictions for the coherent source are in good agreement with experimental calibrations, proving that our detection model accounts for all significant biases. We can therefore confidently interpret the molecular SPS photon statistics we measure. For our SPS, the number of two-photon pulses is 10 times smaller than the corresponding probability for a Poissonian source. As mentioned earlier, residual multi-photon pulses mostly result from background fluorescence light triggered by Ti:Sa excitation. Indeed, the wavelength of this parasitic light lies within the molecule's fluorescence band and therefore cannot be filtered out. Careful optimization of substrate purity as well as of the purity of the chemicals used in sample fabrication can probably lower background fluorescence.

3.3. Molecular SPS efficiency

Our molecular SPS emission can be modelled as the superposition of a perfect SPS and a coherent state of light. In this model, all sources of linear loss (production + collection

+ detection) are gathered as an overall efficiency η . For this perfect SPS (perf. SPS), the photon probability distribution of light impinging on the APD is then given by

$$\mathcal{P}_{\text{perf.SPS}}^{\text{in}}(0) = 1 - \eta, \quad \mathcal{P}_{\text{perf.SPS}}^{\text{in}}(1) = \eta, \quad \mathcal{P}_{\text{perf.SPS}}^{\text{in}}(n \geq 2) = 0. \quad (9)$$

Background (backgnd.) emission is modelled by a coherent state of light with a mean number $\eta\gamma$ of detected photons per pulse. The corresponding photon probability distribution is then

$$\mathcal{P}_{\text{backgnd.}}^{\text{in}}(n) = \frac{e^{-\eta\gamma}(\eta\gamma)^n}{n!} \quad \text{for } n \geq 0. \quad (10)$$

Applying equations (2)–(4) to the (perf. SPS + backgnd.) probability distribution leads to the following analytical expressions for the real SPS (S) *photocounts* statistics:

$$\begin{aligned} P_S(0) &= e^{-\eta\gamma}(1 - \eta), \\ P_S(1) &= 2(e^{-\eta\gamma/2} - e^{-\eta\gamma}) + \eta(2e^{-\eta\gamma} - e^{-\eta\gamma/2}), \\ P_S(2) &= (1 - e^{-\eta\gamma/2})^2 + \eta(e^{-\eta\gamma/2} - e^{-\eta\gamma}). \end{aligned} \quad (11)$$

Values for collection efficiency η and signal-to-background ratio $1/\gamma$ can be inferred from measured photocount statistics P_S (see table 2). Using equations (11) for experimental values of $P_S(1)$ and $P_S(2)$, we find $\eta \simeq 0.04456$ and $\eta\gamma \simeq 2.02 \times 10^{-3}$. This leads to a signal-to-background ratio of 22, in good agreement with that measured by sample raster scan.

3.4. Single-pulse Mandel parameter

From a statistical point of view, there exist two main differences between experimental and ideal SPS: source overall efficiency < 1 , and finite ratio of single- to multi-photon pulses. Light produced by an ideal SPS consists of the periodic emission and detection of single photons with 100% efficiency. For such a source, there is therefore virtually no noise on the number of photon recorded during any integration time. In the following, we call this absence of intensity noise ‘perfect intensity squeezing’. On the other hand, a real SPS yields non-ideal intensity squeezing [3].

It is then meaningful to assess SPS performance by measuring its intensity noise on the excitation repetition period τ_{rep} timescale [11]. Such analysis requires evaluation of the single-pulse Mandel parameter Q [36]. This parameter characterizes deviation of photon statistics from Poissonian statistics for which $Q = 0$. Sub-Poissonian (resp. super-Poissonian) statistics correspond to $Q < 0$ (resp. $Q > 0$). For the distribution $\{n_p^{(d)}\}$ of detected photon number, the Mandel parameter is defined by

$$Q \equiv \frac{\langle n^2 \rangle - \langle n \rangle^2}{\langle n \rangle} - 1 \equiv \frac{\langle (\Delta n)^2 \rangle}{\langle n \rangle} - 1, \quad (12)$$

where $\langle n \rangle$ stands for the average value of $\{n_p^{(d)}\}$ calculated over the ensemble $\{p\}$ of excitation pulses. Note that an ideal SPS would yield $Q = -1$. Moreover, for any statistical distribution,

the effect of linear attenuation can be straightforwardly evaluated: after linear attenuation η , a Mandel parameter Q_0 would be changed to ηQ_0 . This means that every statistical distribution converges towards Poissonian statistics under attenuation. This sensitivity to loss for measurements of non-zero Mandel parameters is similar to sensitivity observed in ‘standard squeezing experiments’ dealing with CW and pulsed laser beams [37]. In such experiments, photodetection is realized with photodiodes, the output current fluctuations reproducing the intensity fluctuations of the detected beam. Evidence for squeezing is then a measured reduced noise spectra with respect to a calibrated shotnoise reference.

For our molecular SPS, the Mandel parameter Q of the *photoncount* statistics can be computed directly from single-pulse photoncount probabilities

$$Q = [P(1) + 2P(2)] \left\{ \frac{2P(2)}{[P(1) + 2P(2)]^2} - 1 \right\}. \quad (13)$$

From the data of table 2 we infer a Mandel parameter $Q_S = -0.04455$ for the SPS. This negative value for Q confirms that our SPS indeed exhibits sub-Poissonian statistics at the timescale τ_{rep} . Since very few multi-photon events are observed, the value of Q_S is almost only limited by the collection efficiency, which imposes a lower limit on Q : $Q_{\text{limit}} = -\eta = -0.04456$.

Our measurement of Q_S can then be compared with a Poissonian reference measurement. Here again, statistical bias introduced by APD deadtime must be taken into account. From equations (6)–(8) and (13), we can derive the Mandel parameter of detected photons for a coherent source (C) of parameter α . Noticing that $\langle n \rangle_C = 2(1 - e^{-\alpha/2})$, we have

$$Q_C = \langle n \rangle_C \left[\frac{2P_C(2)}{\langle n \rangle_C^2} - 1 \right] = -\frac{\langle n \rangle_C}{2}. \quad (14)$$

As a consequence of photodetector deadtimes, a coherent source gives sub-Poissonian distribution of photodetection events. In our case, a coherent source with the same mean number $\langle n \rangle_C = \langle n \rangle = 0.04653$ of detected photons per pulse as the SPS, would then yield $Q_C = -0.02327 > Q_S$. Despite this detection bias, our direct measurement of the Mandel parameter still yields a value for Q_S that clearly departs from that of Poissonian statistics. This *measured* Mandel parameter is larger (in absolute value) than those measured in previous measurements by more than one order of magnitude [2, 27, 36].

4. SPS intensity fluctuations

Emission intermittency has been observed with most SPSs realized so far [13]–[15]. This effect decreases source efficiency and contributes to additional source of noise. Better understanding of physical processes responsible for intermittency would probably lead to significant improvement of current SPS devices.

To characterize intermittency for our molecular SPS, we have investigated its influence on the photon statistics recorded with the time-resolved photon counting system. For a periodically triggered SPS, this analysis is equivalent to studying the source intensity noise over a wide range of timescales, which is usually done in the frequency domain for ‘standard squeezing experiments’ [37], using a radio-frequency spectrum analyser.

4.1. Measuring intensity fluctuations: time-varying Mandel parameter $Q(T)$

The analysis performed on single-pulse photon statistics (see section 3.4) can be extended to multiple-pulses scale, allowing characterization of intensity fluctuations at any timescale greater than the pulse repetition period. To do this, we analyse fluctuations of the total number $N(T)$ of photons detected during an integration time $T \equiv \mathcal{M}\tau_{\text{rep}}$, which is a multiple of the repetition period. This analysis therefore corresponds to studying statistics of the photocounts number recorded during \mathcal{M} successive pulses.

We then introduce the time-varying Mandel parameter $Q(T)$ [38], defined similarly to single-pulse Mandel parameter. To perform statistical analysis, we extend the procedure used in section 3. More precisely, the complete data $\{n_p^{(d)}\}_{p=1,\dots,\mathcal{N}}$ corresponding to photocounts recorded during \mathcal{N} consecutive excitation pulses are split in successive samples, each lasting T . We then obtain $\mathcal{N}_{\text{sample}} = E[\mathcal{N}/\mathcal{M}]$ samples. We call $N_k(T)$, the number of photocounts recorded during the k th sample. We then have

$$N_k(T) \equiv \int_{kT}^{(k+1)T} I(t) dt = \sum_{p=k\mathcal{M}}^{(k+1)\mathcal{M}-1} n_p^{(d)}. \quad (15)$$

The statistical average over these samples of duration T is denoted $\langle \rangle_T$, and we hence have

$$\langle N \rangle_T = \frac{1}{\mathcal{N}_{\text{sample}}} \sum_{k=0}^{\mathcal{N}_{\text{sample}}-1} N_k(T). \quad (16)$$

Using these notations, the time-dependent Mandel parameter is given by

$$Q(T) \equiv \frac{\langle (\Delta N)^2 \rangle_T}{\langle N \rangle_T} - 1, \quad (17)$$

which allows direct comparison of SPS noise properties with those of Poissonian light beam.

4.2. Intensity noise and intermittency in the molecular fluorescence: the ON–OFF model

To analyse our experimental results and link them to physical parameters of molecular fluorescence, we use a simple analytical model of molecular intermittency, in which we assume that the SPS can be ON or OFF. We call p the ON to OFF transition rate and q the OFF to ON one. These rates correspond to lifetimes $\tau_{\text{on}} = 1/p$ and $\tau_{\text{off}} = 1/q$, respectively.

4.2.1. Physical interpretation of the ON–OFF model. For molecular SPS [11] and other SPSs relying on fluorescence of a single emitter (e.g. single NV centres in diamond nanocrystals [14]), ON–OFF intermittency stems from the presence of a metastable non-fluorescent excited state in the energy level structure. Dynamics of ON–OFF behaviour can then be computed from the three-level structure shown in figure 4.

- ON \rightarrow OFF transition corresponds to relaxation from the optical excited state S_1 to the triplet state T_1 . For each excitation cycle, the probability \mathcal{P}_{ISC} of this intersystem crossing process is very small in the case of the DiIC₁₈(3) molecule used in our experiment ($\mathcal{P}_{\text{ISC}} \simeq 10^{-4}$).

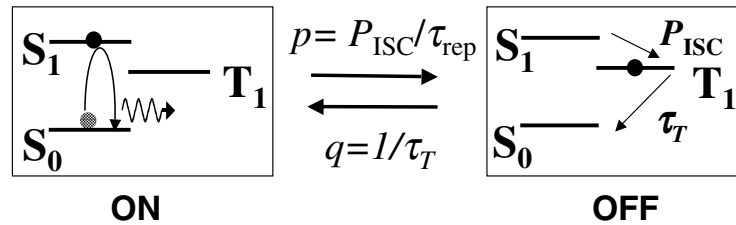


Figure 4. Three-state energy level structure and the corresponding ON and OFF states in the SPS intermittency model. In the ON state, the molecule undergoes fluorescent cycles between the ground S_0 and excited S_1 singlet states. In the OFF state, the molecule is trapped in the dark metastable triplet T_1 state. Coupling from S_1 to T_1 occurs at each excitation pulse with the intersystem crossing probability \mathcal{P}_{ISC} , yielding a transition ON \rightarrow OFF rate $p = \mathcal{P}_{\text{ISC}}/\tau_{\text{rep}}$. The reverse transition OFF \rightarrow ON occurs at rate $q = 1/\tau_T$, where τ_T is the triplet-state lifetime.

Moreover, since singlet–triplet transitions occur exclusively from the excited state S_1 , the excitation repetition period must be considered in defining the source ON state lifetime τ_{on} , which is then $\tau_{\text{on}} = \tau_{\text{rep}}/\mathcal{P}_{\text{ISC}}$, assuming saturated excitation regime.

- OFF \rightarrow ON transition consists simply of non-radiative decay from triplet T_1 to ground S_0 state. Note that the triplet level is metastable since selection rules forbid direct optical transition to the ground state. The triplet-state lifetime $\tau_T = \tau_{\text{off}} = 1/q$ is therefore usually much longer than a typical fluorescent lifetime (in the case of DiIC₁₈(3), $\tau_T \simeq 200 \mu\text{s}$ [35]).

4.2.2. Dynamics of the ON–OFF system. Under periodic pulsed excitation, the ON–OFF dynamics can be described using a discrete-time model. As transitions between ON and OFF states are random, we introduce a stochastic variable r_k to account for the source state at instants $t_k = k\tau_{\text{rep}}$. This parameter has value $r_k = 1$ (resp. $r_k = 0$) if the source is in the ON (resp. OFF) state at time t_k .

We then call u_k the probability for the source to be in the ON state at time t_k . As the SPS emits photons exclusively from the ON state and never from the OFF state, u_k also corresponds to the photoemission probability at time t_k . We assume that lifetimes τ_{on} and τ_{off} of the ON–OFF states are much larger than the repetition rate τ_{rep} . Then, the ON \rightarrow OFF transition probability is $p\tau_{\text{rep}}$ and the OFF \rightarrow ON transition is $q\tau_{\text{rep}}$. It follows that the state of the emitter at pulse $k + 1$ depends only on its state at pulse k . The recursion relation for the probability u_{k+1} of the source to be ON at time t_{k+1} is

$$u_{k+1} = (1 - p\tau_{\text{rep}})u_k + q\tau_{\text{rep}}(1 - u_k), \quad (18)$$

which leads to the general solution

$$u_k = \left(u_0 - \frac{q}{p+q} \right) (1 - p\tau_{\text{rep}} - q\tau_{\text{rep}})^k + \frac{q}{p+q}. \quad (19)$$

Stationary probabilities for the molecule to be either ON or OFF are then

$$P_{\text{on}} = \frac{q}{(p+q)}, \quad (20)$$

$$P_{\text{off}} = 1 - P_{\text{on}} = \frac{p}{(p+q)}. \quad (21)$$

4.2.3. Source intensity and Mandel parameter versus time. According to our model, light emitted by the source is a succession of single photon pulses emitted at time $t_k = k\tau_{\text{rep}}$ with probability u_k , corresponding to an intensity

$$I(t) = \sum_{k=-\infty}^{+\infty} \delta(t - k\tau_{\text{rep}}) r_k \quad \text{with } r_k = 0 \text{ or } 1. \quad (22)$$

The recursive relation (19) for the ON–OFF model permits computation of statistical properties of source intensity $I(t)$. In particular, we can derive the time-dependent Mandel parameter from the variance of the number $N(T)$ of photons emitted by the intermittent source during $T = \mathcal{M}\tau_{\text{rep}}$. Details of this calculation are given in appendix B.

Analytical expression of the Mandel parameter given by equation (B.13) can be simplified in the regime for which $\beta = (p+q)\tau_{\text{rep}} \ll 1$, leading to the following Mandel parameter expression for a ‘perfect’ SPS with intermittency:

$$Q_{\text{perf.SPS}}(\mathcal{M}\tau_{\text{rep}}) = \frac{2p\tau_{\text{rep}}}{\beta^2} \left\{ 1 - \frac{1}{\mathcal{M}\beta} [1 - (1-\beta)^{\mathcal{M}}] \right\} - 1. \quad (23)$$

Experimental measurements of the Mandel parameter are also affected by overall efficiency $\eta < 1$ (see section 3.3). Taking into account this limitation which is equivalent to linear loss, the Mandel parameter of the real source $Q_S(T)$ is given by

$$Q_S(T) = \eta Q_{\text{perf.SPS}}(T). \quad (24)$$

4.2.4. Experimental data analysis. As shown in figure 5, our experimental data are well-fitted by equations (23) and (24) over more than four orders of magnitude in time. Setting the measured efficiency to $\eta = 0.04456$, the fit yields $p\tau_{\text{rep}} = \mathcal{P}_{\text{ISC}} = 2.1 \times 10^{-4}$ and $\tau_T = 250 \mu\text{s}$, for the remaining two free parameters. These values are in good agreement with values given in [35].

Figure 5 clearly shows that source photon statistics differ on short and long timescales. On timescales shorter than $\simeq 8\tau_{\text{rep}}$, the Mandel parameter of the source $Q(T)$ is smaller than Q_C , the theoretical value of the Mandel parameter for Poissonian light including the detection deadtime (broken horizontal line in figure 5). On this short timescale, the SPS’s photocount statistics are those of non-classical light. On timescales larger than $\simeq 10 \mu\text{s}$, fluorescence intermittency due to the triplet state influences the photocount statistics by introducing excess of noise resulting in a positive value of the Mandel parameter.

The model developed here for a perfect intermittent SPS fits our experimental data with good accuracy. Indeed, apart from detection loss, other imperfections can be ignored or handled

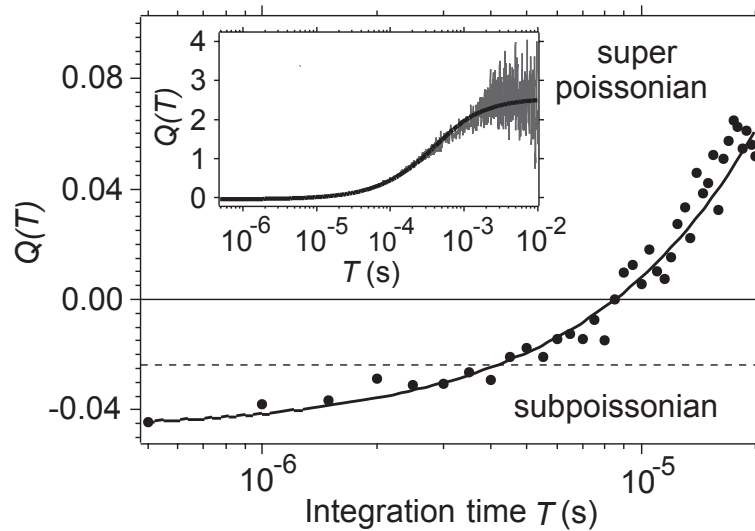


Figure 5. Direct measurement of Mandel parameter $Q(T)$ over short integration time T . The broken horizontal line shows $Q(T)$ for the equivalent coherent source (C), taking into account detection dead time. The inset shows $Q(T)$ for longer integration time. The solid curve is a fit given by the model accounting for intermittency in SPS emission.

by the following:

- Since the repetition period τ_{rep} is much longer than the photodetection deadtime and since multi-photon events are extremely rare with our SPS, APD deadtime does not alter significantly the photocount statistics. The detection can be considered effectively linear and equation (24) remains valid in the presence of detection deadtimes.
- High signal-to-background ratio means that background light does not contribute significantly to photocount statistics. It can therefore be neglected, as done implicitly in the model developed in this section. It can, moreover, be shown that addition of uncorrelated Poissonian background light of intensity B to the perfect SPS signal S is equivalent to loss. If we model the real source by the superposition of fluorescence background and light from a perfect SPS, then, introducing $\rho \equiv S/(S+B)$, the Mandel parameter of the real source is simply given by $Q_{S+B} = \rho Q_S$.

4.2.5. SPS intensity autocorrelation function. As a consistency check for our study, the time-dependent Mandel parameter analysis can be compared with a different approach using the intensity autocorrelation function $g^{(2)}$ [39], the measurement of which being at the heart of fluorescence correlation spectroscopy [40]. In particular, one can readily establish (see appendix C) that the area of the zero delay peak normalized to a coherent source, called $g^{(2)}(0)$, is related to the single-pulse Mandel parameter Q , by

$$Q = \langle n \rangle \left(\frac{g^{(2)}(0)}{2} - 1 \right). \quad (25)$$

Due to technical limitations, it was however not possible to record simultaneously the timestamps and the histogram of time delays between consecutive photodetections. Nevertheless, $g^{(2)}(0)$ and Q can be extracted from the set of photocount timestamps to check the validity of equation (25), as shown in appendix C. From the measured single-pulse Mandel parameter, equation (25) predicts $g^{(2)}(0) = 0.085$, whereas direct calculation of the autocorrelation function yields $g^{(2)}(0) = 0.082$, in very good agreement with the ‘predicted’ value. These values of $g^{(2)}(0)$ and Q , measured at the level of a single pulse, are the signature of specific quantum features of the SPS.

Molecular photodynamics on longer timescales (a few hundred μs to ms) can be inferred from measurements of the time dependence of the intensity autocorrelation function. Taking into account the specificity of the pulsed excitation regime, we introduce a discrete-time autocorrelation function for time delay $\Delta \times \tau_{\text{rep}}$ given by

$$G^{(2)}(\Delta) \equiv \frac{\langle n_i n_{i+\Delta} \rangle}{\langle n_i \rangle^2}, \quad (26)$$

where n_i is the number of detected photons in the i th excitation pulse, and Δ is an integer.

This discrete correlation function is directly related to the intensity autocorrelation function $g^{(2)}(\tau) \equiv \langle I(t)I(t+\tau) \rangle / \langle I(t) \rangle^2$ usually measured with start–stop techniques [12]. It can be shown that the normalized area of the k th peak (with the 0th reference peak corresponding to $\tau = 0$) of $g^{(2)}(\tau)$ over a period τ_{rep} is equal to $G^{(2)}(\Delta = k)$.

The ON–OFF model developed in section 4 can be applied to calculate $G^{(2)}(\Delta)$:

$$G^{(2)}(\Delta) = \frac{p}{q} e^{-(p+q)\Delta \times \tau_{\text{rep}}}, \quad (27)$$

which coincides with the formula given in [15].

From our data $\{n_p^{(d)}\}$, we numerically compute $G^{(2)}(\Delta)$, varying Δ from 1 to 1000. Note that the latter value is chosen because blinking occurs in a timescale range of $\simeq 1000\tau_{\text{rep}}$. Results of this $G^{(2)}(\Delta)$ calculation are displayed in figure 6. The experimental curve is fitted with equation (27), providing another way of measuring dynamical parameters of intermittent molecular SPS. This fit yields $\mathcal{P}_{\text{ISC}} = 1.6 \times 10^{-4}$ and $\tau_{\text{T}} = 180 \mu\text{s}$, which are in good agreement with the values obtained in section 4.2.4 using Mandel parameter analysis.

Note that, on the short timescale, the statistical noise is higher on $G^{(2)}$ than on Q . This is due to the fact that $G^{(2)}$ is computed over fewer but bigger statistical samples.

5. Conclusion

We have realized an efficient triggered SPS relying on the temporal control of a single-molecule fluorescence. After a comparison with Poissonian coherent light pulses with the same mean number of photons per pulse, we have characterized intensity noise properties of this SPS in the time domain and photocounting regime.

From the record of every photocount timestamp, we calculate the second-order correlation function $G^{(2)}$ or equivalently the time-dependent Mandel parameter $Q(T)$. Observed negative $Q(T)$ values signify non-classical photocount statistics.

This time-domain analysis is complementary to fluorescent correlation spectroscopy techniques for investigating photochemical properties at the single-emitter level. More

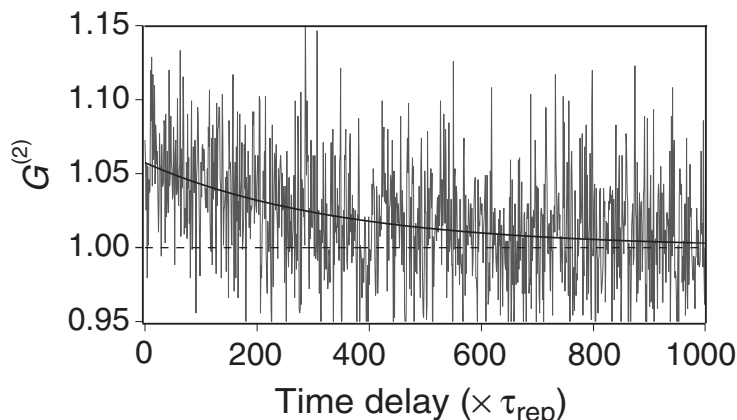


Figure 6. Discrete-time photocount autocorrelation function $G^{(2)}$, computed from the set of data $\{n_p^{(d)}\}$ studied, in the range of time delay $T = 1 \times \tau_{\text{rep}}$ to $T = 1000 \times \tau_{\text{rep}}$. The broken horizontal line corresponds to the shotnoise reference value.

specifically, we have modelled fluorescence intermittency by a two-state ON \leftrightarrow OFF dynamical process. By fitting a theoretical analytical expression of the Mandel parameter for an intermittent SPS, we obtained quantitative values for relevant molecular photodynamical parameters. Such a direct time-domain statistical analysis could give insight into molecular properties such as conformational changes [41, 42], resonant energy transfer [43] or collective emission effects in multichromophoric systems [44].

With expected application to quantum cryptography, higher overall efficiency within a given emission spectral band should be reached so that SPSs can exhibit advantages over attenuated laser pulses [6, 7]. In recent experiments, we coupled the fluorescence of a single emitter (a coloured centre in a diamond nanocrystal) to the single mode of a planar microcavity and observed a significant increase in spectral density of the emitted photons. These preliminary results are a promising realization of an efficient SPS well suited for open-air quantum key distribution.

Acknowledgments

The authors are grateful to V Le Floc’h, L T Xiao and C Grossman for their contributions at various point in the experiment. We also thank P Grangier and J Zyss for fruitful discussions, and Robin Smith for her valuable remarks on the paper. The experimental set-up was built, thanks to the great technical assistance of A Clouqueur, J-P Madrang and C Ollier. This work was supported by an ‘ACI Jeune chercheur’ grant from Ministère de la Recherche, and by a France Télécom R&D grant (‘CTI Télécom Quantique’).

Appendix A. General analysis technique of a set of photocounts

A set of data consists of a list of timestamps $\{t_i\}$ recorded by the TIA computer board. Here we describe the method developed to process raw data. This procedure allows us first to

postsynchronize the timestamps on an excitation timebase and then to build the set $\{n_p^{(d)}\}$ of the number of detected photons for each excitation pulse p .

The pulsed excitation laser acts as a periodic trigger of emitted photons with repetition period $\tau_{\text{rep}} \simeq 488$ ns. An excitation laser pulse is emitted at time $t_{\text{start}} + p\tau_{\text{rep}}$, where the pulse is indexed by the integer p . The parameter t_{start} represents the pulse emission time taken as the first ($p = 0$) of the data. For each set of data, t_{start} and τ_{rep} must be determined because the repetition period of the Ti:Sa fs laser can fluctuate slightly between acquisitions. However, the laser repetition rate is stable over the typical acquisition duration ($< s$), and τ_{rep} is therefore constant for a given data record.

Single-photon emission by the molecule occurs at each excitation pulse after a random time delay related to the molecule's excited state lifetime. Non-synchronous photocounts due to APD dark counts are rare, so almost all recorded photocounts are triggered by photons emitted by the molecule, with few by photons from residual fluorescence background. For these reasons, t_{start} and τ_{rep} can then be determined directly from recorded data.

The i th photocount timestamp t_i can be expressed as

$$t_i = t_{\text{start}} + (p_i \tau_{\text{rep}}) + \delta\tau_i, \quad (\text{A.1})$$

where integer $p_i \in \{1, \dots, \mathcal{N}\}$ indexes the laser pulse preceding detection of the i th photon, and data to be analysed lasts \mathcal{N} repetition periods; $\delta\tau_i$ is the time delay between excitation pulse and photocount timestamp ($0 \leq \delta\tau_i < \tau_{\text{rep}}$). Given a set of timestamps $\{t_i\}$, relevant information can be equivalently represented by lists $\{p_i\}$ and $\{\delta\tau_i\}$, provided the value of τ_{rep} is known accurately enough. Since the fluorescence lifetime of the molecule is much shorter than the laser repetition period, $\delta\tau_i \ll \tau_{\text{rep}}$, as long as photocount i is not a dark count, which is rarely the case.

As the laser period τ_{rep} is not known precisely, we first attempt to synchronize the data on the excitation timebase considered as a clock of period τ_{clock} close to the expected laser period. We introduce a delay function parametrized with t_{start} and τ_{clock} , which gives for each timestamp t_i the time delay between this timestamp and the corresponding top of the clock

$$\text{Delay}_{t_{\text{start}}, \tau_{\text{clock}}}(t_i) = t_i - t_{\text{start}} - E\left(\frac{t_i - t_{\text{start}}}{\tau_{\text{clock}}}\right) \tau_{\text{clock}}, \quad (\text{A.2})$$

where $E()$ stands for the integer part function and, if the clock period differs from the laser period, the drift of the time delay baseline with the pulse index p_i is linear as can be seen in figure A.1(a),

$$\text{Delay}_{t_{\text{start}}, \tau_{\text{clock}}}(t_i) \simeq p_i(\tau_{\text{rep}} - \tau_{\text{clock}}). \quad (\text{A.3})$$

From the slope of the delay function baseline, we infer a new value for τ_{clock} . Note that the first guess for τ_{clock} is usually so far from the laser period that the delay function takes a saw-toothed shape, each jump corresponding to the delay reaching a multiple value of τ_{clock} . As a consequence, only a linear fraction of the sample corresponding to a single saw tooth can be used at first. In further steps, estimation of τ_{rep} improves and fewer jumps occur. Longer samples, corresponding to higher fit precision can then be processed. This procedure is repeated

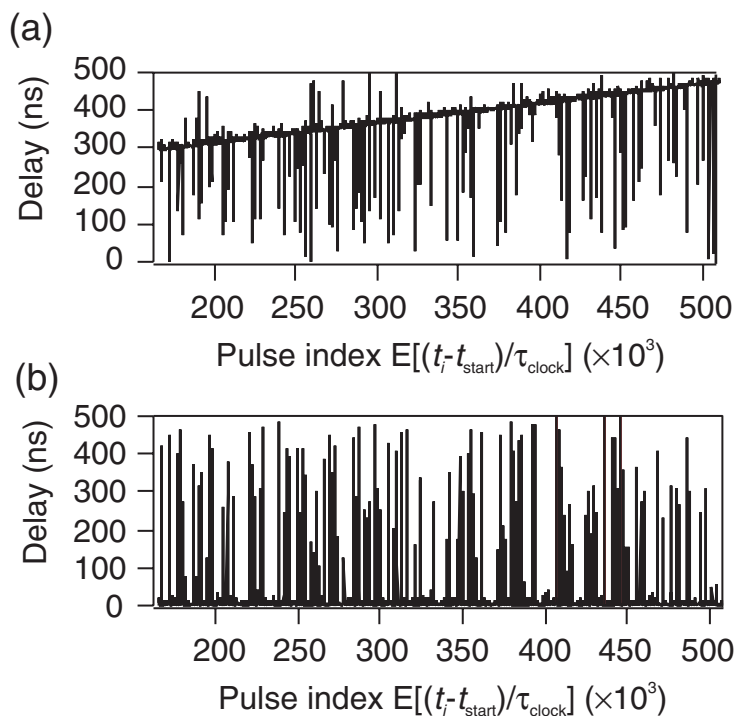


Figure A.1. Synchronization procedure of timestamps $\{t_i\}$, showing delay function $\text{Delay}(t_i)$ versus pulse index $E[(t_i - t_{\text{start}})/\tau_{\text{clock}}]$ for a given set of parameters t_{start} and τ_{clock} . (a) A small linear drift of delay baseline, when τ_{clock} is close to τ_{rep} but t_{start} is incorrect. (b) When $\tau_{\text{clock}} = \tau_{\text{rep}}$ within relative precision of 10^{-9} and t_{start} is properly estimated.

until the whole data set is used, leading to the situation of figure A.1(b). It corresponds to the same fraction of data as in figure A.1(a), for which τ_{rep} is determined up to relative precision greater than 10^{-9} .

Once τ_{rep} and t_{start} values are known, calculation of the lists $\{p_i\}$ and $\{\delta\tau_i\}$ is straightforward using

$$p_i = E\left(\frac{t_i - t_{\text{start}}}{\tau_{\text{rep}}}\right) \quad \text{and} \quad \delta\tau_i = \text{Delay}_{t_{\text{start}}, \tau_{\text{rep}}}(t_i). \quad (\text{A.4})$$

A time-filtering procedure is then used to eliminate all photocounts with time delay much longer than the molecular excited-state lifetime. To implement this filter, we use a time window of duration ΔT_{window} . From the set $\{p_i\}$, we calculate the number n_i of photons detected by the two photodiodes in the time interval $[p_i\tau_{\text{rep}}, p_i\tau_{\text{rep}} + \Delta T_{\text{window}}]$. The time window duration ΔT_{window} must be shorter than the laser period and much longer than the molecular excited-state lifetime $1/\Gamma$ so that the probability of discarding a ‘real’ photodetection event is negligible. The chosen time window duration $\Delta T_{\text{window}} = 30$ ns meets these two conditions, considering $1/\Gamma \simeq 2.5$ ns for DiIC₁₈(3) dye. Note that the choice of a time window significantly shorter than the laser period has the advantage of filtering out our data from the majority of non-synchronous background photocounts, such as APD dark counts.

The processed data, now expressed as the table $\{n_i, p_i\}$, and shortened to $\{n_p^{(d)}\}$ in the body of this paper, allows us to characterize the statistics of our source on timescales from $\tau_{\text{rep}} \simeq 500$ ns to ms.

Appendix B. Statistical characterization of an intermittent SPS

Here, we derive a general analytical expression of the ‘perfect’ intermittent SPS Mandel parameter $Q(T)$ defined by equation (17) using the ON–OFF model introduced in section 4.2. We also retrieve the approximate expression (23) for $Q(T)$. We assume that source emission has reached its steady state at time $t = 0$.

The total number $N(T)$ of photocounts recorded during an integration time $T = \mathcal{M}\tau_{\text{rep}}$ corresponding to \mathcal{M} consecutive excitation pulses is related to the stochastic photocount variable r_k associated with the k th excitation pulse (see section 4.2.3) by

$$N(T) = \sum_{k=0}^{\mathcal{M}-1} r_k. \quad (\text{B.1})$$

Calculating $Q(T)$ is equivalent to evaluating the variance $\langle N^2 \rangle_T - \langle N \rangle_T^2$, where mean values $\langle \rangle_T$ are defined by equation (16). Both $\langle N \rangle_T$ and $\langle N^2 \rangle_T$ should then be evaluated. The mean value of $N(T)$ is given by

$$\langle N \rangle_T = \sum_{k=0}^{\mathcal{M}-1} \langle r_k \rangle = \mathcal{M} \frac{q}{p+q}, \quad (\text{B.2})$$

where the steady-state expression of $\langle r_k \rangle = q/(p+q)$ comes from the definition of r_k and the recursive law (19). Similarly, $\langle N^2 \rangle_T$ follows

$$\langle N^2 \rangle_T = \sum_{k=0}^{\mathcal{M}-1} \sum_{k'=0}^{\mathcal{M}-1} \langle r_k r_{k'} \rangle. \quad (\text{B.3})$$

Index change $\ell = |k - k'|$ in the previous equation then yields

$$\langle N^2 \rangle_T = \sum_{k=0}^{\mathcal{M}-1} \langle r_k^2 \rangle + 2 \sum_{k=0}^{\mathcal{M}-1} \sum_{\ell=1}^{\mathcal{M}-k} C(\ell) = \sum_{k=0}^{\mathcal{M}-1} \langle r_k \rangle + 2 \sum_{\ell=1}^{\mathcal{M}-1} (\mathcal{M} - \ell) C(\ell), \quad (\text{B.4})$$

where we have introduced the discrete-time *correlation function* $C(\ell)$ defined as

$$C(\ell) = \langle r_k r_{k+\ell} \rangle - \langle r_k \rangle \langle r_{k+\ell} \rangle. \quad (\text{B.5})$$

Calculation of $Q(T)$ now relies on evaluation of $C(\ell)$. We recall that, in the model of section 4.2, source dynamics is described by stochastic process u_k , the probability for the molecular system to be in the ON state. The general expression of $u_{k+\ell}$ follows from the recursive law (19):

$$u_{k+\ell} = \left(u_k - \frac{q}{p+q} \right) (1 - p\tau_{\text{rep}} - q\tau_{\text{rep}})^\ell + \frac{q}{p+q}. \quad (\text{B.6})$$

The stochastic variable $r_k = 1$ if the state is ON with probability u_k , and 0 if the state is OFF with probability $1 - u_k$. The product $r_k r_{k+\ell}$ is then equal to 1 only if both r_k and $r_{k+\ell}$ are simultaneously equal to 1 and otherwise equal to 0. It can be summarized as

$$\langle r_k r_{k+\ell} \rangle = P(r_k = 1)P(r_{k+\ell} = 1 | r_k = 1), \quad (\text{B.7})$$

$$\langle r_k \rangle \langle r_{k+\ell} \rangle = P(r_k = 1)P(r_{k+\ell} = 1). \quad (\text{B.8})$$

Note that $P(r_k = 1)$ is the probability that $r_k = 1$, and $P(r_{k+\ell} = 1 | r_k = 1)$ is the conditional probability for $r_{k+\ell} = 1$ when $r_k = 1$. To fulfil this latter condition $r_k = 1$, one needs to have $u_k = 1$. Moreover, by definition, the steady-state probability is $P(r_k = 1) = q/(p + q)$, so that we have

$$P(r_{k+\ell} = 1 | r_k = 1) = \frac{p}{p + q} (1 - p\tau_{\text{rep}} - q\tau_{\text{rep}})^\ell + \frac{q}{p + q}, \quad (\text{B.9})$$

and, as a consequence,

$$C(\ell) = \frac{pq}{(p + q)^2} (1 - p\tau_{\text{rep}} - q\tau_{\text{rep}})^\ell. \quad (\text{B.10})$$

This value $C(\ell)$ is then introduced into equation (B.4), and the expression for the variance follows from (B.4) and (B.2):

$$\langle N^2 \rangle_T - \langle N \rangle_T^2 = \frac{pq}{(p + q)^2} \left[\mathcal{M} \frac{1 + \alpha}{1 - \alpha} - 2\alpha \frac{1 - \alpha^{\mathcal{M}}}{(1 - \alpha)^2} \right], \quad (\text{B.11})$$

where $\alpha \equiv (1 - p\tau_{\text{rep}} - q\tau_{\text{rep}})$.

The general analytical expression of the ‘perfect’ intermittent SPS Mandel parameter is finally deduced by

$$Q_{\text{perf.SPS}}(\mathcal{M}\tau_{\text{rep}}) = \frac{\langle N^2 \rangle_T - \langle N \rangle_T^2}{\langle N \rangle_T} - 1 \quad (\text{B.12})$$

$$= \frac{p}{p + q} \left(\frac{2 - \beta}{\beta} - \frac{2(1 - \beta)}{\mathcal{M}} \cdot \frac{1 - (1 - \beta)^{\mathcal{M}}}{\beta^2} \right) - 1, \quad (\text{B.13})$$

where $\beta \equiv (p + q)\tau_{\text{rep}}$. In the limit of $\beta \ll 1$, which is the case for molecular system dynamics considered in the body of this paper, we retrieve expression (23).

Appendix C. Histogram of time delays from the set of photocounts

The record of the emission timestamps for our SPS contains all information necessary to derive the histogram of the time delays between photodetections on the two detectors of the Hanbury

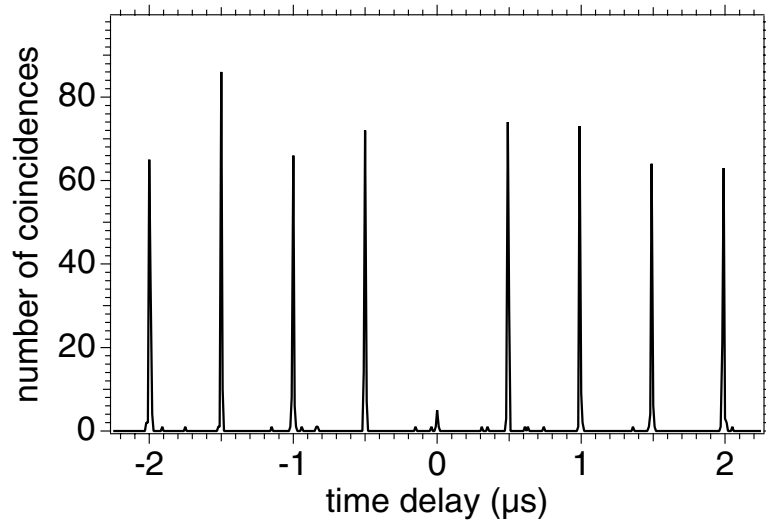


Figure C.1. Histogram of time delays computed in the vicinity of zero delay, from the two detector timestamp sequences. The bin time per channel was set to 10 ns.

Brown and Twiss set-up. These data are usually acquired with a start–stop technique, relying on a time-to-amplitude converter and a multichannel analyser. In the limit of low collection efficiency and short timescale, it coincides with the second-order intensity correlation function $g^{(2)}$ [32].

The most usual statistical characterization of a SPS relies in the measurement of ‘ $g^{(2)}(0)$ ’, standing for the area of the $g^{(2)}$ function around zero time delay, normalized to the counts one would expect in the case of an equivalent coherent source. We have computed the histogram of the time delays from the set of timestamps on each detector to check for the consistency of the single-pulse Mandel parameter measurement with that of $g^{(2)}(0)$. Figure C.1 displays this computed histogram.

Indeed, both Mandel and $g^{(2)}(0)$ parameters are linked to the photocounts probability distribution $P(0, 1, 2)$. In a start–stop measurement, one would expect

$$g^{(2)}(0) = \frac{P(2)}{\langle n/2 \rangle^2} = \frac{4P(2)}{(P(1) + 2P(2))^2}, \quad (\text{C.1})$$

which yields for the SPS studied $g^{(2)}(0) = 8.5 \times 10^{-2}$. Hence, comparing with equation (13) we recall equation (25):

$$Q = \langle n \rangle \left(\frac{g^{(2)}(0)}{2} - 1 \right).$$

If we normalize the number of coincidences around zero time delay in a 500 ns time window to an equivalent coherent source we obtain $g^{(2)}(0) = 8.2 \times 10^{-2}$. This result is consistent with the value of 8.5×10^{-2} inferred from equation (25).

References

- [1] Kimble H J, Dagenais M and Mandel M 1977 *Phys. Rev. Lett.* **39** 691
- [2] Diedrich F and Walther H 1987 *Phys. Rev. Lett.* **58** 203
- [3] Imamoğlu A and Yamamoto Y 1994 *Phys. Rev. Lett.* **72** 210
- [4] Kim J, Benson O, Kan H and Yamamoto Y 1999 *Nature* **397** 500
- [5] Laflamme L, Knill E and Milburn G J 2001 *Nature* **409** 46
- [6] Beveratos A, Brouri R, Gacoin T, Villing A, Poizat J-P and Grangier P 2002 *Phys. Rev. Lett.* **89** 187901
- [7] Waks E, Inoue K, Santori C, Fattal D, Vučković J, Solomon G and Yamamoto Y 2002 *Nature* **420** 762
- [8] Lütkenhaus N 2000 *Phys. Rev. A* **61** 052304
- [9] De Martini F, Di Giuseppe G and Marrocco M 1996 *Phys. Rev. Lett.* **76** 900
- [10] Brouri R, Beveratos A, Poizat J-P and Grangier P 2000 *Phys. Rev. A* **62** 063814
- [11] Treussart F, Alléaume R, Le Floc'h V, Xiao L T, Courty J-M and Roch J-F 2002 *Phys. Rev. Lett.* **89** 093601
- [12] Brunel C, Lounis B, Tamarat P and Orrit M 1999 *Phys. Rev. Lett.* **83** 2722
- [13] Lounis B and Moerner W M 2000 *Nature* **407** 491
- [14] Beveratos A, Kühn S, Brouri R, Gacoin T, Poizat J P and Grangier P 2002 *Eur. Phys. J. D* **18** 191
- [15] Santori C, Pelton M, Solomon G, Dale Y and Yamamoto Y 2001 *Phys. Rev. Lett.* **86** 1502
- [16] Moreau E, Robert I, Gérard J-M, Abram I, Manin L and Thierry-Mieg V 2001 *Appl. Phys. Lett.* **79** 2865
- [17] Santori C, Fattal D, Vučković J, Solomon G and Yamamoto Y 2002 *Nature* **419** 594
- [18] Pelton M, Santori C, Vučković J, Zhang B, Solomon G, Plant J and Yamamoto Y 2002 *Phys. Rev. Lett.* **89** 233602
- [19] Hours J, Varoutsis S, Gallart M, Bloch J, Robert-Philip I, Cavanna A, Abram I, Laruelle F and Gérard J-M 2003 *Appl. Phys. Lett.* **82** 2206
- [20] Vučković J, Fattal D, Santori C, Solomon G and Yamamoto Y 2003 *Appl. Phys. Lett.* **82** 3596
- [21] Zwiller V, Aichele T, Seifert W, Persson J and Benson O 2003 *Appl. Phys. Lett.* **82** 1509
- [22] Sebald K, Michler P, Passow T, Hommel D, Bacher G and Forchel A 2002 *Appl. Phys. Lett.* **81** 2920
- [23] Strauf S, Michler P, Klude M, Hommel D, Bacher G and Forchel A 2002 *Phys. Rev. Lett.* **89** 177403
- [24] Yuan Z, Kardynal B E, Stevenson R M, Shields A J, Lobo C J, Cooper K, Beattie N S, Ritchie D A and Pepper M 2002 *Science* **295** 102
- [25] Kuhn A, Hennrich M and Rempe G 2002 *Phys. Rev. Lett.* **89** 067901
- [26] Kurtsiefer C, Mayer S, Zarda P and Weinfurter H 2000 *Phys. Rev. Lett.* **85** 290
- [27] Fleury L, Segura J M, Zumofen G, Hecht B and Wild U 2000 *Phys. Rev. Lett.* **84** 1148
- [28] Treussart F, Clouqueur A, Grossman C and Roch J F 2001 *Opt. Lett.* **26** 1504
- [29] Atkins P W and Friedman R S 1997 *Molecular Quantum Mechanics* (Oxford: Oxford University Press)
- [30] Loudon R 2000 *The Quantum Theory of Light* (Oxford: Oxford University Press)
- [31] Grangier P, Roger G and Aspect A 1986 *Europhys. Lett.* **1** 173
- [32] Reynaud S 1983 *Ann. Phys. Fr.* **8** 315
- [33] Brouri R, Beveratos A, Poizat J-P and Grangier P 2000 *Opt. Lett.* **25** 1294
- [34] Eggeling C, Widengren J, Rigler R and Seidel C 1998 *Anal. Chem.* **70** 2651
- [35] Veerman J A, Garcia-Parajo M F, Kuipers L and Van Hulst N F 1999 *Phys. Rev. Lett.* **83** 2155
- [36] Short R and Mandel L 1983 *Phys. Rev. Lett.* **51** 384
- [37] Bachor H A 1998 *A Guide to Experiments in Quantum Optics* (Weinheim: Wiley-VCH)
- [38] Mandel L 1979 *Opt. Lett.* **4** 205
- [39] Bernard J, Fleury L, Talon H and Orrit M 1993 *J. Chem. Phys.* **98** 850
- [40] Chu B 1991 *Laser Light Scattering. Basic Principles and Practice* (Boston, MA: Academic)

- [41] Yang H and Xie X S 2002 *Chem. Phys.* **284** 423
Yang H, Luo G, Karnchanaphanurach P, Louie T-M, Rech I, Cova S, Xun L and Xie X S 2003 *Science* **302** 262
- [42] Barsegov V and Mukamel S 2002 *J. Chem. Phys.* **116** 9802
- [43] Berglund A, Doherty A and Mabuchi H 2002 *Phys. Rev. Lett.* **89** 068101
- [44] Hübner C G, Zumofen G, Renn A, Herrmann A, Müllen K and Basché T 2003 *Phys. Rev. Lett.* **91** 093903